Supporting Information

Polyoxomolybdate–polypyrrole / reduced graphene oxide nanocomposite as high capacity electrodes for lithium storage

Mi Zhang,[a]† Tao Wei,[ab]† A-Man Zhang,[a] Shun-Li Li,[a] Feng-Cui Shen,[c] Long-Zhang Dong,[a] Dong- ShengLi [d] and Ya-Qian Lan*[a]

[a]Jiangsu Key Laboratory of Biofunctional Materials, College of Chemistry and Materials Science, Nanjing Normal University, Nanjing 210023, P. R. China

E-mail: yqlan@njnu.edu.cn

[b]School of Energy and Power, Jiangsu University of Science and Technology, Zhenjiang 212003, P. R. China

[c]College of Biological and Chemical Engineering,Anhui Polytechnic University, Wuhu 241000, P. R. China

[d]School of Materials and Chemical Engineering, Key Laboratory of Inorganic Nonmetallic Crystalline and Energy Conversion Materials, China Three Gorges University, Yichang 443002, P. R.China.

†These authors contribute equally to this work.

Table of Contents

I.	Raman spectra and FT-IR spectra of the samples	-S3-
II.	FE-SEM image and TEM image of the samples	-S3-
III.	HAADF-STEM image and the corresponding EDS mapping of PMo_{12}/RGO	-S4-
IV.	Nitrogen adsorption isotherms and the pore size distribution of the samples	-S4-
V.	TGA results of PMo_{12} and PMo_{12}-PPy/RGO	-S4-
VI.	XPS spectra of PMo_{12}-PPy/RGO before and after discharged to 0.01 V	-S5-
VII.	Cycle-life performance and Rate capability test of the samples	-S6-
VIII.	Cycle-life performance and Rate capability test of the samples	-S6-
IX.	Cycling performance of PMo_{12}-PPy/RGO at 2.0 A g^{-1}	-S6-
X.	FESEM image of the samples before and after 50 cycles	-S7-
XI.	Comparison of PMo_{12}-PPy/RGO with other POMs-based anodes	-S8-

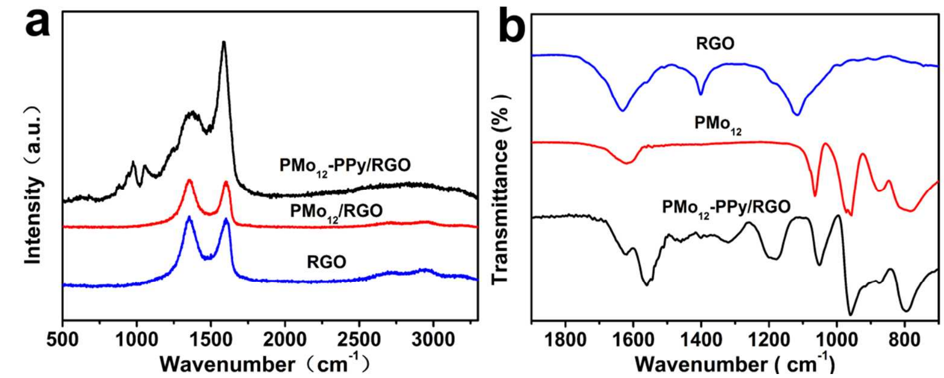

Figure S1. (a) Raman spectra of PMo_{12}-PPy/RGO, PMo_{12}/RGO, and pure RGO, respectively. (b) FT-IR spectra of PMo_{12}-PPy/RGO, PMo_{12}, and pure RGO, respectively.

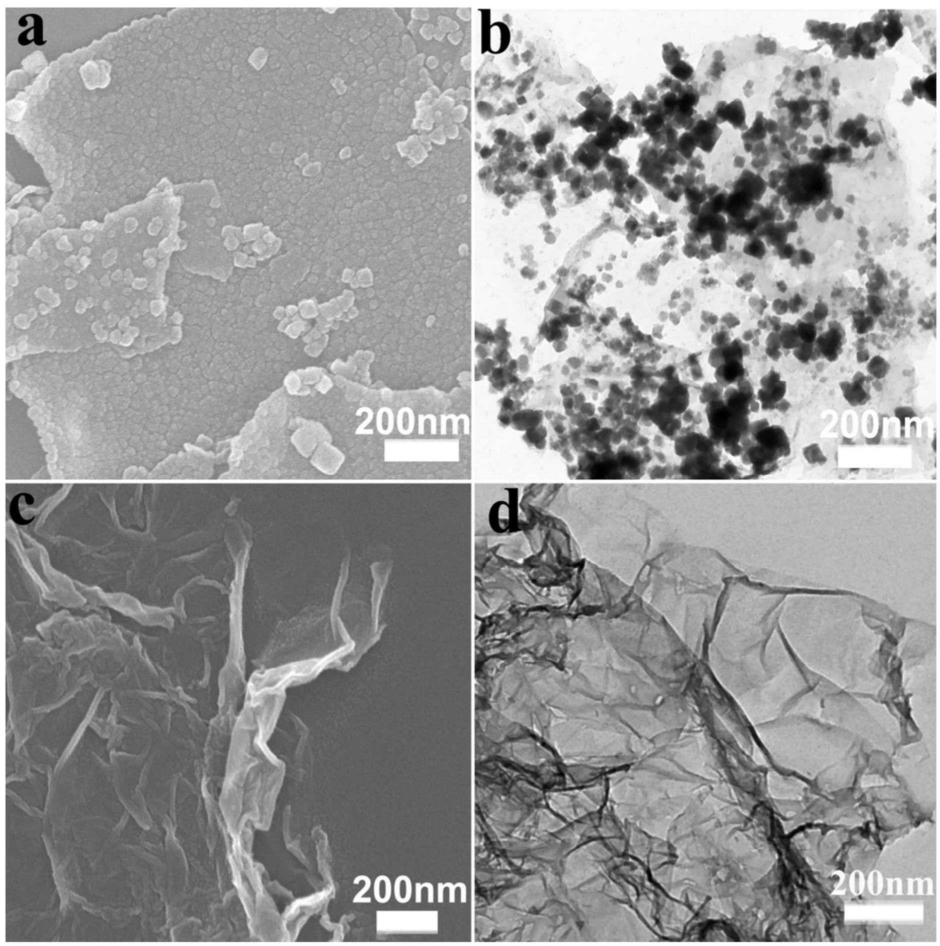

Figure S2. (a) FE-SEM image of $CoMo_6$-PPy/RGO. (b) TEM image of $CoMo_6$-PPy/RGO. (c) FE-SEM image of PMo_{12}/RGO. (d) TEM image of PMo_{12}/RGO.

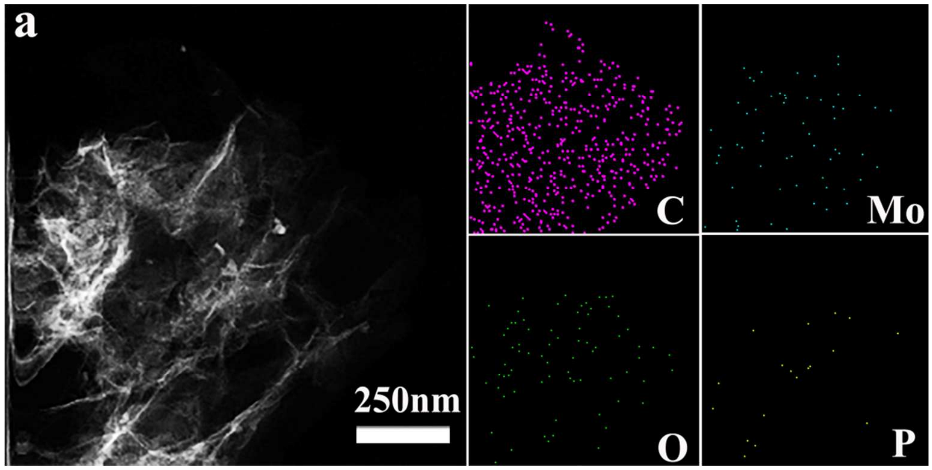

Figure S3. (a) HAADF-STEM image of PMo_{12}/RGO and the corresponding EDS mapping of C, Mo, O and P elements, respectively.

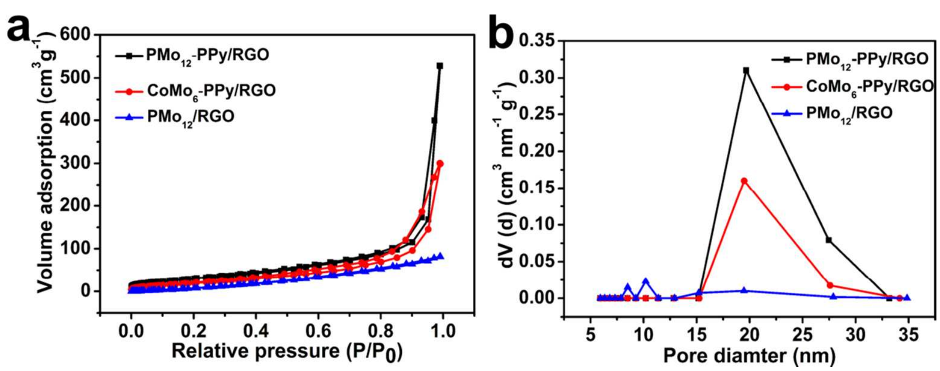

Figure S4. (a) Nitrogen adsorption-desorption isotherms of PMo_{12}-PPy/RGO, PPy-$CoMo_6$/RGO, PMo_{12}/RGO, respectively. (b) The pore size distribution of the above samples by BJH method.

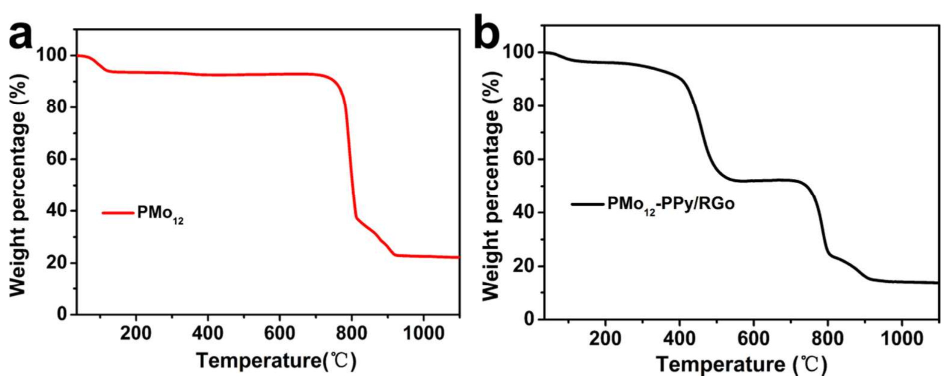

Figure S5. (a) TGA results of PMo_{12} and (b) PMo_{12}-PPy/RGO in O_2 (10 □ min^{-1}).

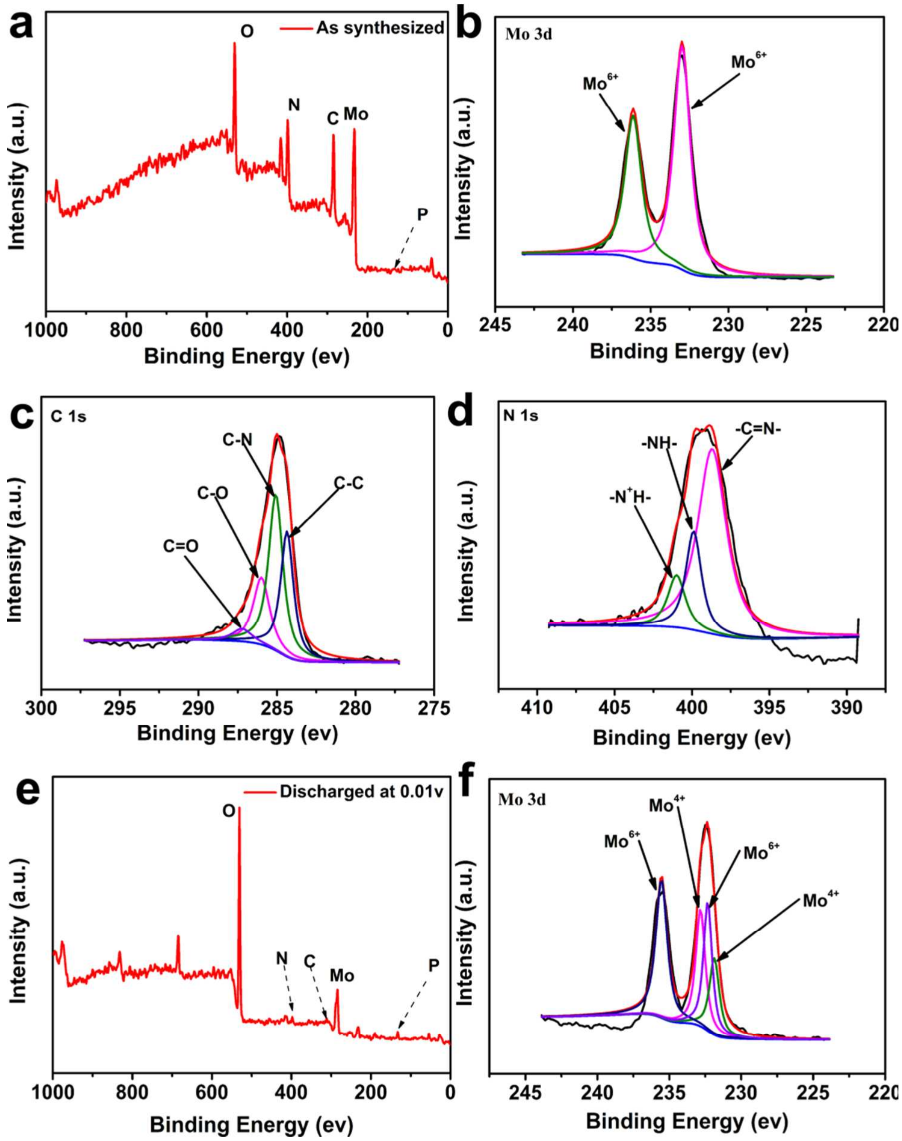

Figure S6. XPS spectra of PMo_{12}-PPy/RGO before and after discharged to 0.01 V. (a-d): As-synthesized powder. (a) As-synthesized powder survey scan, (b) Mo 3d, (c) C 1s, (d) N 1s, respectively. (e-f): Discharged at 0.01 V, (e) survey scan (f) Mo 3d, respectively.

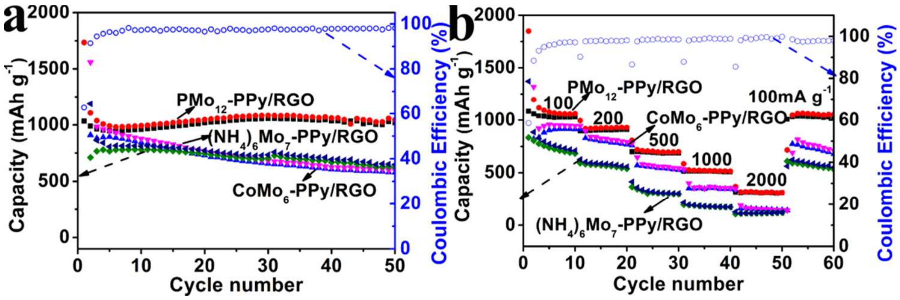

Figure S7. (a) Cycle-life performance of PMo_{12}-PPy/RGO, $CoMo_6$–PPy/RGO and $(NH_4)_6Mo_7$–PPy/RGO at a current density of 100 mA g^{-1}. (b) Rate capability test for the PMo_{12}-PPy/RGO, $CoMo_6$–PPy/RGO and $(NH_4)_6Mo_7$–PPy/RGO at various current densities (100–2000 mA g^{-1}).

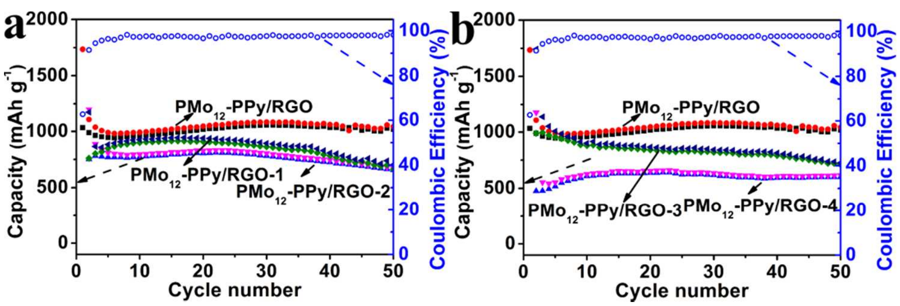

Figure S8. (a) Cycle-life performance of PMo_{12}-PPy/RGO, PMo_{12}-PPy/RGO-1 and PMo_{12}-PPy/RGO-2 at a current density of 100 mA g^{-1}. (b) Cycle-life performance of PMo_{12}-PPy/RGO, PMo_{12}-PPy/RGO-3 and PMo_{12}-PPy/RGO-4 at a current density of 100 mA g^{-1}.

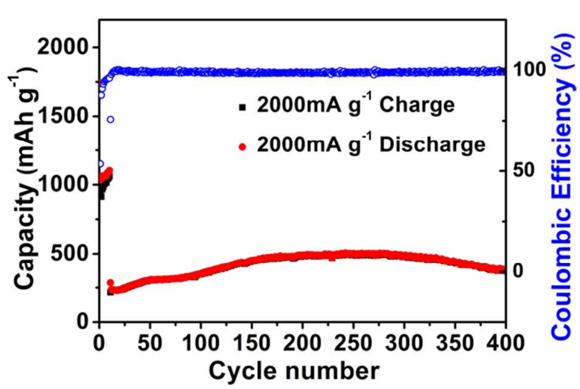

Figure S9. Cycling performance of PMo_{12}–PPy/RGO at 2.0 A g^{-1} after a few cycles at 100 mA g^{-1}.

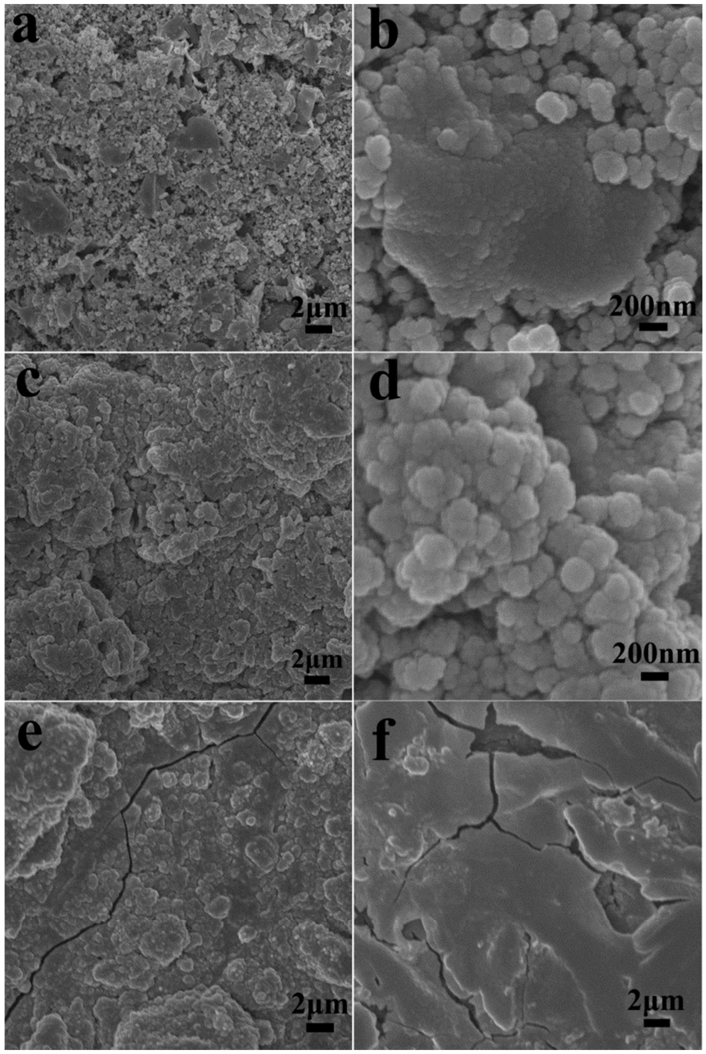

Figure S10. FESEM images of (a, b) PMo_{12}–PPy/RGO electrode before and (c, d) PMo_{12}–PPy/RGO (e) $CoMo_6$–PPy/RGO (f) $(NH_4)_6Mo_7$–PPy/RGO electrode after 50 cycles performed with a current density of 1.0 A g^{-1}.

Table S1. Comparison of PMo_{12}-PPy/RGO with other POMs-based anodes

Materials	CR(mA g^{-1})	RC(mAh g^{-1})	AR (%)	Ref.
PMo_{12}-PPy/RGO	100	1082	70	This work
NAM-EDAG	100	Above 1000	80	1
$[MnMo_6O_{24}]^{9-}$/SWNTs	0.5 $mAcm^{-2}$	932	50	2
Pyrene-Anderson-CNTs	0.5 $mAcm^{-2}$	665	30	3
Mo_6O_{18}-SCN	50	876	40	4
SiW_{11}– CNTs	0.5 $mAcm^{-2}$	650	30	5
Py–SiW_{11}/SWNTs	0.5 $mAcm^{-2}$	580	30	6
POMOF-1	500	350	65	7

CR: Charge rate. RC: Reversible capacity. AR: Active material ratio.

Calculation of the theoretical capacities.

The theoretical capacities were calculated according to the equation:

$$Q = \frac{nF}{3.6M} = \frac{96500n}{3.6M} \cdots (1)$$

Where Q is the reversible charging–discharging capacity, n is the number of electrons passed during the redox reaction, and M is the molecular weight.

POM: When Li^+ intercalate/ deintercalate into the structure of PMo_{12}, we have a hypothesis that the redox reactions of Mo^{6+} can be changed to Mo^{4+} or Mo^0. So, $n_{(maximum)}$= 72, $Q_{(POM\ maximum)}$ = 1057.38 mAh g^{-1}. According to the TGA and experiment, we can calculate the content of the POMs is about 72.9%, $Q_{(PMo12\text{-}PPy/RGO)}$= 1057.38×72.9%=835.16 mAh g^{-1}.

References

(1) Xie, J.; Zhang, Y.; Han, Y.; Li, C., High-Capacity Molecular Scale Conversion Anode Enabled by Hybridizing Cluster-Type Framework of High Loading with Amino-Functionalized Graphene. *ACS Nano* **2016,** *10* (5), 5304-13.

(2) Ji, Y.; Hu, J.; Huang, L.; Chen, W.; Streb, C.; Song, Y.-F., Covalent Attachment of Anderson-Type Polyoxometalates to Single-Walled Carbon Nanotubes Gives Enhanced Performance Electrodes for Lithium Ion Batteries. *Chemistry - A*

European Journal **2015,** *21* (17), 6469-6474.

(3) Huang, L.; Hu, J.; Ji, Y.; Streb, C.; Song, Y. F., Pyrene-Anderson-Modified CNTs as Anode Materials for Lithium-Ion Batteries. *Chemistry* **2015,** *21* (51), 18799-804.

(4) Nasim Khan, R. N.; Mahmood, N.; Lv, C.; Sima, G.; Zhang, J.; Hao, J.; Hou, Y.; Wei, Y., Pristine organo-imido polyoxometalates as an anode for lithium ion batteries. *RSC Advances* **2014,** *4* (15), 7374.

(5) Chen, W.; Huang, L.; Hu, J.; Li, T.; Jia, F.; Song, Y.-F., Connecting carbon nanotubes to polyoxometalate clusters for engineering high-performance anode materials. *Phys. Chem. Chem. Phys.* **2014,** *16* (36), 19668-19673.

(6) Ma, D.; Liang, L.; Chen, W.; Liu, H.; Song, Y.-F., Covalently Tethered Polyoxometalate-Pyrene Hybrids for Noncovalent Sidewall Functionalization of Single-Walled Carbon Nanotubes as High-Performance Anode Material. *Adv. Funct. Mater.* **2013,** *23* (48), 6100-6105.

(7) Yue, Y.; Li, Y.; Bi, Z.; Veith, G. M.; Bridges, C. A.; Guo, B.; Chen, J.; Mullins, D. R.; Surwade, S. P.; Mahurin, S. M.; Liu, H.; Paranthaman, M. P.; Dai, S., A POM–organic framework anode for Li-ion battery. *J. Mater. Chem. A* **2015,** *3* (45), 22989-22995.